

Fig. 4—CaO solubility as a function of P_2O_5 , SiO_2 , and Al_2O_3 concentration in CaF_2 -CaO- P_2O_5 , CaF_2 -CaO- SiO_2 , and Al_2O_3 - CaF_2 -CaO melts.

dependence of CaO solubility on the concentrations of P_2O_5 , SiO_2 , and Al_2O_3 in $CaF_2 \cdot CaO$ - P_2O_5 , $CaF_2 \cdot CaO \cdot SiO_2$, and $Al_2O_3 \cdot CaF_2$ -CaO melts is shown in Figure 4. Addition of these oxides increases the solubility of CaO. Maximum solubility is 65, 56, and 41 at compositions saturated with $CaO \cdot 3CaO \cdot P_2O_5$, $CaO \cdot 3CaO \cdot SiO_2$, and $CaO \cdot 11CaO \cdot 7Al_2O_3 \cdot CaF_2$, respectively. The CaO solubility increases linearly with the increase in the SiO_2 or Al_2O_3 added. In the CaF_2 -CaO- P_2O_5 system, the substitution of P_2O_5 for CaF_2 increases the solubility of CaO markedly above 15 mass pct P_2O_5 . That means some part of CaF_2 can be substituted by P_2O_5 .

The standard free energy change of formation $4CaO \cdot P_2O_5$ is reported.^[7] At liquidus saturated with CaO and $4CaO \cdot P_2O_5$, the activities of CaO and $4CaO \cdot P_2O_5$ are unity. Therefore, the activity of P_2O_5 in the composition referred to pure solid P_2O_5 is calculated as 4.3×10^{-43} . The phase relations show high solubility of P_2O_5 and low activity of P_2O_5 at the liquidus saturated with CaO and $4CaO \cdot P_2O_5$. Effective dephosphorization would be conducted with the slag in the region of three phases equilibria: liquidus, CaO, and $4CaO \cdot P_2O_5$.

Isothermal phase relations for the CaF_2 -CaO- P_2O_5 system were investigated by a chemical equilibration technique at 1623 K and the following conclusions were drawn:

1. In the low CaF_2 region of the system at 1623 K, the liquid contains 20 to 30 mass pct P_2O_5 and is surrounded by the primary phase fields of CaO, $4CaO \cdot P_2O_5$, and $CaF_2 \cdot 9CaO \cdot 3P_2O_5$.
2. The liquid of this system at the composition of CaO and $4CaO \cdot P_2O_5$ doubly saturated is the most effective for dephosphorization.

REFERENCES

1. A. Tagaya, H. Chiba, F. Tsukihashi, and N. Sano: *Metall. Trans. B*, 1991, vol. 22B, pp. 499-502.

2. J. Berak and I. Tomczak-Hudyma: *Rocz. Chem.*, 1972, vol. 46, pp. 2157-67.
3. M. Maeda and Y. Kariya: *Iron Steel Inst. Jpn. Int.*, 1993, vol. 33, pp. 182-87.
4. N. Nakashima, K. Hayashi, Y. Ohta, and K. Morinaga: *Mater. Trans. JIM*, 1991, vol. 32, pp. 37-42.
5. S. Ueda and M. Maeda: *Metall. Mater. Trans. B*, 1999, vol. 30B, pp. 921-25.
6. S. Ueda, K. Takemoto, T. Ikeda, and M. Maeda: *Iron Steel Inst. Jpn. Int.*, 2000, vol. 40, pp. s92-s95.
7. A. Tagaya, F. Tsukihashi, and N. Sano: *Trans. ISS*, 1991, pp. 63-69.
8. J. Mukerji: *J. Am. Ceram. Soc.*, 1965, vol. 48 (4), pp. 210-13.
9. A.K. Chatterjee and G.I. Zhmoldin: *J. Mater. Sci.*, 1972, vol. 7, pp. 93-97.

Effect of Constitutional Supercooling on the Numerical Solution of Species Concentration Distribution in Laser Surface Alloying

SUMAN CHAKRABORTY, SUPRIYA SARKAR, and PRADIP DUTTA

Laser surface alloying (LSA) is the process of localized heating of an elemental layer of a substrate by means of laser and a simultaneous feeding of the alloying element over the molten surface in order to achieve desirable surface properties, without affecting the bulk properties of the base material. It has been generally perceived that convection is a dominant mechanism of transport of the added species inside the molten pool,^[1] and, hence, has a much bigger role to play in the overall alloying process than species diffusion. This may lead to a situation in which the role of the species diffusion coefficient may be overlooked or underestimated. In addition, accurate numerical values of the same are hardly available for a wide range of material combinations. In such situations, it is possible that an inaccurate value of the species diffusion coefficient may lead to unrealistic solutions for the final species concentration distribution. It can be noted that, in this context, species concentration is defined as the ratio of the mass of the alloying element (species) to the total mass inside a particular control volume. Hence, in all practical situations, if the concentration (mass fraction) of the added species in any control volume exceeds unity, as obtained from a numerical simulation, it is bound to be unrealistic. In the present article, we attempt to investigate the role of the species diffusion coefficient in this regard, an issue often neglected in numerical simulations.

Figure 1 shows a schematic diagram of a typical laser surface alloying process. As shown in the figure, a laser beam moving with a constant scanning speed (u_{scan}) in the horizontal direction and having a defined power distribution strikes the surface of an opaque material, and a part of the energy is absorbed. A thin melt pool forms on the surface due to laser

SUMAN CHAKRABORTY, Research Fellow, Department of Mechanical Engineering, Indian Institute of Science, is Lecturer, on leave from the Department of Power Plant Engineering, Jadavpur University, Calcutta - 700098, India. SUPRIYA SARKAR, Graduate Student, and PRADIP DUTTA, Assistant Professor, are with the Department of Mechanical Engineering, Indian Institute of Science, Bangalore - 560012, India.

Manuscript submitted February 15, 2001.

heating. Simultaneously, a powder of a different material is fed into the pool, which mixes with the molten substrate by convection and diffusion. As the laser source moves away from a location, resolidification of the zone occurs, leading to a final microstructure of the alloyed surface.

The governing equations for mass, momentum, energy, and species transport can be cast in a general conservative form as

$$\frac{\partial(\rho\phi)}{\partial t} + \nabla \cdot (\rho \mathbf{u} \phi) = \nabla \cdot (\Gamma \nabla \phi) + S \quad [1]$$

where ϕ is a general scalar variable, Γ is an equivalent diffusion coefficient, \mathbf{u} is the continuum velocity vector, and S is a general source term. Equation [1] is written with respect to a stationary coordinate system (x - y - z). However, the problem is more conveniently studied in a reference frame fixed with the laser (x' - y' - z'). To achieve this purpose, the following transformation can be used:^[2]

$$x = x' - u_{\text{scan}} t \quad [2]$$

Using the preceding transformation, the governing equations in the moving coordinate system are written as^[2]

Continuity:

$$\frac{\partial \rho}{\partial t} + \nabla \cdot \mathbf{u} = 0 \quad [3]$$

Momentum conservation:

$$\frac{\partial}{\partial t} (\rho \mathbf{u}) + \rho \mathbf{u} \cdot (\nabla \mathbf{u}) = \nabla \cdot (\mu_L \frac{\rho}{\rho_L} \nabla \mathbf{u}) - \nabla p + S_b - A \mathbf{u} \quad [4]$$

where

$$S_b = \rho \mathbf{g} [\beta_T (T - T_0) + \beta_C (C_L - C_0)]$$

In Eq. [4] ρ is the density; p is the pressure; μ is the viscosity; and β_T and β_C are coefficients of thermal and solutal volumetric expansion, respectively. The subscript L refers to the liquid phase. The coefficient A (to be described later) is essentially a function that ensures a smooth transition from zero velocity in the solid phase to a fully developed velocity field in the liquid phase.

Energy conservation:

$$\begin{aligned} \frac{\partial}{\partial t} (\rho T) + \nabla \cdot (\rho \mathbf{u} T) &= \nabla \cdot \left(\frac{k_T}{c_p} \nabla T \right) - \frac{1}{c_p} \frac{\partial}{\partial t} (\rho \Delta H) \\ - \nabla \cdot \left(\frac{\rho}{c_p} \mathbf{u} \Delta H \right) &- \frac{\partial}{\partial x} \left(\rho u_{\text{scan}} \left(T + \frac{\Delta H}{c_p} \right) \right) \end{aligned} \quad [5]$$

where T is the temperature, c_p is the specific heat, k_T is the thermal conductivity, and ΔH is the latent enthalpy.

Species conservation:

$$\frac{\partial}{\partial t} (\rho C_L) + \nabla \cdot (\rho \mathbf{u} C_L) = \nabla \cdot (\rho D_L \nabla C_L) - \frac{\partial}{\partial x} (\rho u_{\text{scan}} C_L) \quad [6]$$

Regarding the boundary conditions, at the top surface, we employ a heat balance as follows:

$$-q''(r) + h(T - T_\infty) + \sigma_\epsilon \epsilon (T^4 - T_\infty^4) = -k \frac{\partial T}{\partial y} \quad [7]$$

where σ_ϵ is the Stefan Boltzman constant, ϵ is the emissivity

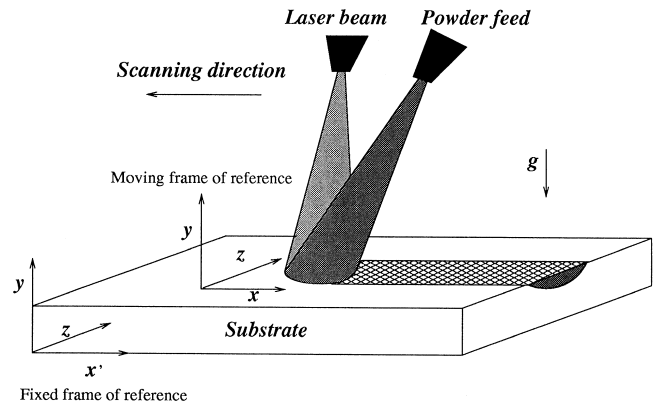


Fig. 1—A schematic diagram of the physical problem.

of the top surface, and $q''(r)$ is expressed as a Gaussian heat distribution at the top surface; *i.e.*,

$$q''(r) = \frac{Q}{\pi r_q^2} \exp\left(-\frac{r^2}{r_q^2}\right) \quad [8]$$

In the preceding equation, Q is the net energy input (*laser power* \times *efficiency*) and r_q is the radius of heat input. The top surface is assumed to be flat (*i.e.*, $v = 0$). Also, at the top surface, the Marangoni convection leads to a shear stress balance expressed as

$$\tau_{yx} = -\mu \left(\frac{\partial u}{\partial y} \right)_h = \frac{\partial \sigma}{\partial T} \left(\frac{\partial T}{\partial x} \right)_h \quad [9]$$

$$\tau_{yz} = -\mu \left(\frac{\partial w}{\partial y} \right)_h = \frac{\partial \sigma}{\partial T} \left(\frac{\partial T}{\partial z} \right)_h \quad [10]$$

where σ is the surface tension; and u , v , and w are the velocity components along the x , y , and z directions, respectively. The bottom of the workpiece is assumed to be insulated. The sides are subjected to heat loss by convection to the ambient.

The three-dimensional governing equations of mass, momentum, and energy conservation (Eq. [3] through [6]) are simultaneously solved numerically using a pressure-based semi-implicit finite volume technique according to the SIMPLER algorithm.^[3] The algorithm is appropriately modified to include the enthalpy-porosity model^[4] for the phase change occurring during the alloying process. The term A in Eq. [4] is modeled using the Kozeny-Carman relationship^[4] as

$$A = a \frac{(1 - f_l)^2}{f_l^3 + b} \quad [11]$$

where a is a large number in accordance with the morphology of a porous medium, b is a small number to avoid division by zero, and f_l is the liquid fraction defined as $\Delta H/L$. In the numerical solution of the energy conservation equation, a special treatment is applied to update the nodal latent heat content,^[4,5] so that the difference in temperature solved from the energy equation and that predicted by phase change considerations is effectively neutralized. Convergence in the inner iterations is declared on the basis of the relative error of scalar variables to be solved (a tolerance of 10^{-4} is prescribed), as well as on the satisfaction of the overall energy balance criteria within a permissible limit of 0.1 pct.

The formulation for solution of species conservation is briefly outlined as follows. In each time-step, the species conservation equation (Eq. [6] is solved after solving the momentum and energy equations. At the top surface, the mass flux of the alloying element (aluminum, in this case) is modeled as a Neumann boundary condition:

$$-D_L \frac{\partial C_L}{\partial y} = \dot{m} \quad [12a]$$

where \dot{m} is the mass flux of aluminum distributed uniformly over a circular area of radius r_q . The mass flux, \dot{m} , is assumed to be uniform and is calculated from the powder feed rate, m_f , as

$$\dot{m} = \left(\frac{m_f}{\pi r_q^2} \right) \quad [12b]$$

The alloying element mixes with the molten base metal by convection and diffusion. At the solidification interface, only a part of the solute, kC_L , goes into the solid phase, where k is the partition coefficient. This happens because the solute is less soluble in the solid phase than in the liquid phase. As a result, the remaining solute, $(1 - k)C_L$, is rejected back into the liquid. Thus, the solute flux balance at the solidification front is given by^[1]

$$-D_L \frac{\partial C_L}{\partial n} = R(C_L)(1 - k) \quad [13]$$

where n is the direction of the outward normal and R is the interface velocity in that direction. At the fusion front, the melting solid does not contain the alloying element, which results in an effective dilution of the solute. The resulting boundary condition at the fusion front can be written as^[1]

$$D_L \frac{\partial C_L}{\partial n} = -R(C_L) \quad [14]$$

In order to obtain the concentration distribution inside the laser-molten pool, one has to solve the macroscopic species conservation equation (Eq. [6]). A natural boundary condition in this regard, consistent with the physical process presently under consideration, is a mass flux boundary condition at the top (Eq. [12]), since alloying elements are generally added at a specified rate at the top surface. Boundary conditions along the solidification and melting interfaces, too, are in the form of mass fluxes. Under such conditions, the steady-state solution of such an equation is capable of yielding concentration values only up to a constant, and thereby cannot give us the absolute concentration distribution. On the other hand, the solution of a transient species conservation equation with a specified initial condition can yield a unique concentration distribution in the solidified alloy. However, in order to adjudge whether that unique solution is physically realistic, a deeper physical insight is required into the dynamics of stable planar front growth during an alloy solidification process.

In order to focus our attention on solidification during laser surface alloying, we first note that, during resolidification of a previously molten pool (once the laser source passes away), a solute-rich boundary layer builds up in the vicinity of the solidifying planar interface, on account of solute rejection from the solid into the liquid. Depending on certain morphological factors, this planar interface can become stable or unstable. In practice, if the actual temperature of the

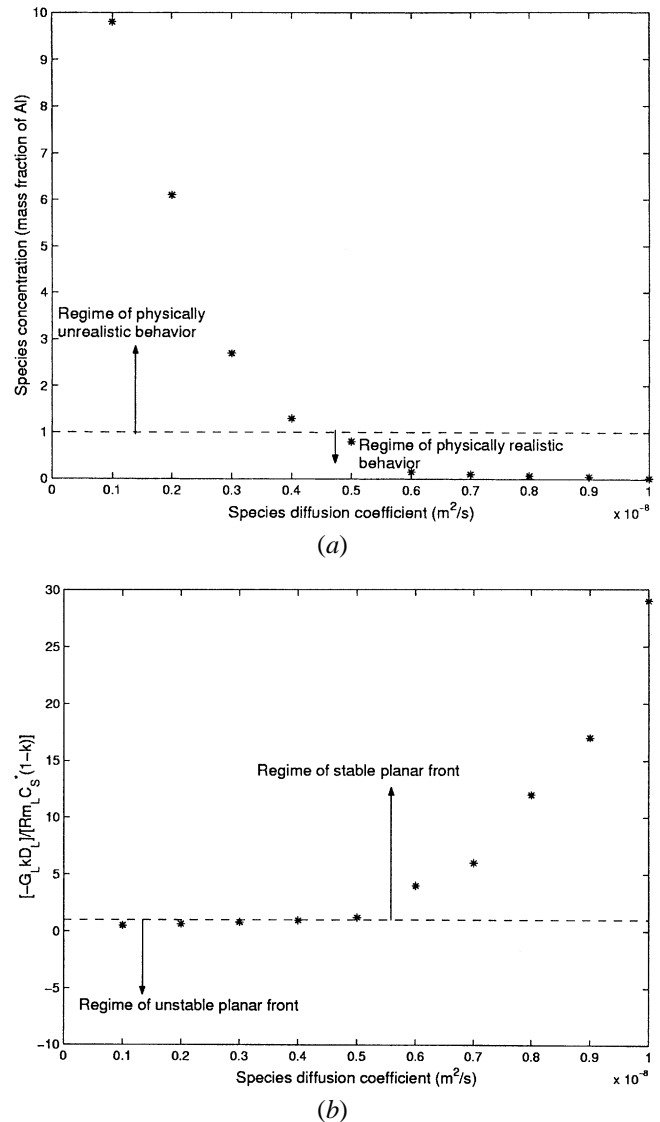


Fig. 2—(a) Variation of maximum species concentration in the solidified alloy (mass fraction of aluminum) with a species mass diffusion coefficient in the liquid used for numerical simulation. (b) Regimes of unstable and stable planar front propagation against the species mass diffusion coefficient in the liquid used for numerical simulation.

liquid immediately in front of the interface is below the equilibrium liquidus temperature, then any protuberance forming on the interface would be in a supercooled liquid state and, therefore, would not disappear. From this constitutional supercooling criterion, the condition for the existence of a planar stable front can be mathematically written as^[6]

$$\frac{G_L}{R} \geq -\frac{m_L C_s^* (1 - k)}{k D_L} \quad [15]$$

where G_L is the thermal gradient at the liquid at the interface, R is the rate of movement of the interface, and m_L is the slope of the liquidus line in the phase diagram. The term C_s^* is the solute concentration in the solid at the interface, D_L is the diffusion coefficient of the added species in the molten state, and k is the equilibrium partition coefficient defined as

$$C_s^* = k C_L^* \quad [16]$$

Using a three-dimensional transient model for LSA, we aim to further investigate whether an arbitrary choice of diffusion coefficient (D_L) is capable of resulting in an unstable planar front (by violation of Eq. [14]), and thereby giving rise to unrealistic values (more than unity) of species concentration, even when the numerical model is otherwise appropriate.

Numerical simulations are carried out with aluminum as the alloying element and iron as the base metal. The thermo-physical properties are assumed to be functions of temperature and are taken from *Smithel's Handbook*.^[7] The process parameters appropriate for the simulated problem are $Q = 2400$ W, $r_q = 0.8$ mm, $m_f = 2 \times 10^{-5}$ kg/s, $u_{scan} = 0.017$ m/s, and the efficiency of heat input = 0.22. In order to adjudge the effect of D_L on the species concentration field numerically obtained, we solve the problem with different values of D_L , keeping values of all other parameters unaltered.

Figures 2(a) and (b) show the variation of maximum

species concentration and the ratio $\frac{-G_L}{R}$, respectively, with species diffusion coefficient. As obtained from Eq. [15], the solidification front moves as a stable planar front when the preceding ratio is more than unity. As we decrease D_L , the right-hand side of Eq. [15] increases. Finally, when D_L goes below 5×10^{-9} m²/s (approximately), the ratio becomes less than unity (refer to Figure 2(b)). Accordingly, it can be inferred that, for the present problem, with a diffusion coefficient less than 5×10^{-9} m²/s (approximately), solidification takes place with an unstable planar front. Such instability can be manifested in numerical solutions also, giving rise to physically unrealistic values of the numerically solved species concentration in the solidified alloy. Figure 2(a) clearly shows that when D_L is chosen to be less than about 4.5×10^{-9} m²/s (which is very close

to the approximate limiting value of 5×10^{-9} m²/s), the maximum concentration value shoots above unity, which is not realistic. A physical explanation for this phenomenon in the numerical simulation may be provided as follows. If the diffusion coefficient is below a certain value, the rejected solute at the solidification interface cannot get transported to the bulk melt quickly enough, leading to a momentary accumulation of solute in the control volume(s) adjacent to the interface. This may result in a value of solute concentration shooting above unity, unless the numerical algorithm has the provision to check this forcibly. Hence, the accuracy of the numerical solution of species concentration distribution in laser surface alloying depends on a constitutional supercooling criterion, which, in turn, depends on whether appropriate values of D_L are used in the simulation in order to satisfy conditions of propagation of a stable planar solidification front. It can be noted that a sensitivity of numerical results on the species diffusion coefficient is also mentioned in the study of He *et al.*^[1] In practice, an improper value of the diffusion coefficient may result in erroneous concentration distributions, even when there is no problem with the numerical algorithm otherwise.

REFERENCES

1. X. He, B.L. Mordike, N. Pirch, and E.W. Kreutz: *Lasers Eng.*, 1995, vol. 4, pp. 291-316.
2. P. Dutta, J. Joshi, and R. Janaswami: *Num. Heat Transfer A*, 1995, vol. 27, pp. 499-518.
3. S.V. Patankar: *Numerical Heat Transfer and Fluid Flow*, Hemisphere, Washington, DC, 1980.
4. A.D. Brent, V.R. Voller, and K.J. Reid: *Num. Heat Transfer*, 1988, vol. 13, pp. 297-318.
5. S. Chakraborty and P. Dutta: *Metall. Mater. Trans. B*, 2001, vol. 32B, pp. 562-64.
6. M.C. Flemings: *Solidification Processing*, McGraw-Hill, New York, NY, 1974.
7. E.A. Brandes: *Smithels Metals Reference Book*, Butterworth and Co. Ltd., London, 1983.